Journal of Polymers and the Environment (2023) 31:870–885
https://doi.org/10.1007/s10924-022-02615-x

ORIGINAL PAPER

Preparation and In Vitro Osteogenic Evaluation of Biomimetic Hybrid Nanocomposite Scaffolds Based on Gelatin/Plasma Rich in Growth Factors (PRGF) and Lithium-Doped 45s5 Bioactive Glass Nanoparticles

Ahmad Reza Farmani[1,2,3] · Mohammad Hossein Nekoofar[1,4,5] · Somayeh Ebrahimi-Barough[1] · Mahmoud Azami[1] · Sohrab Najafipour[2,6] · Somayeh Moradpanah[7] · Jafar Ai[1]

Accepted: 26 September 2022 / Published online: 5 November 2022

Abstract

Bone tissue engineering is an emerging technique for repairing large bone lesions. Biomimetic techniques expand the use of organic–inorganic spongy-like nanocomposite scaffolds and platelet concentrates. In this study, a biomimetic nanocomposite scaffold was prepared using lithium-doped bioactive-glass nanoparticles and gelatin/PRGF. First, sol–gel method was used to prepare bioactive-glass nanoparticles that contain 0, 1, 3, and 5%wt lithium. The lithium content was then optimized based on antibacterial and MTT testing. By freeze-drying, hybrid scaffolds comprising 5, 10, and 20% bioglass were made. On the scaffolds, human endometrial stem cells (hEnSCs) were cultured for adhesion (SEM), survival, and osteogenic differentiation. Alkaline phosphatase activity and osteopontin, osteocalcin, and Runx2 gene expression were measured. The effect of bioactive-glass nanoparticles and PRGF on nanocomposites' mechanical characteristics and glass-transition temperature (T_g) was also studied. An optimal lithium content in bioactive glass structure was found to be 3% wt. Nanoparticle SEM examination indicated grain deformation due to different sizes of lithium and sodium ions. Results showed up to 10% wt bioactive-glass and PRGF increased survival and cell adhesion. Also, Hybrid scaffolds revealed higher ALP-activity and OP, OC, and Runx2 gene expression. Furthermore, bioactive-glass has mainly increased ALP-activity and Runx2 expression, whereas PRGF increases the expression of OP and OC genes. Bioactive-glass increases scaffold modulus and T_g continuously. Hence, the presence of both bioactive-glass and nanocomposite scaffold improves the expression of osteogenic differentiation biomarkers. Subsequently, it seems that hybrid scaffolds based on biopolymers, Li-doped bioactive-glass, and platelet extracts can be a good strategy for bone repair.

✉ Jafar Ai
jafar_ai@tums.ac.ir

Ahmad Reza Farmani
ahmadrezafarmani66@gmail.com

Mohammad Hossein Nekoofar
nekoofar@yahoo.com

Somayeh Ebrahimi-Barough
ebrahimi_s@sina.tums.ac.ir

Mahmoud Azami
azamimahmoud@gmail.com

Sohrab Najafipour
sohrabnajafipour@yahoo.com

Somayeh Moradpanah
zmoradpanah@gmail.com

[1] Department of Tissue Engineering, School of Advanced Technologies in Medicine, Tehran University of Medical Sciences, Tehran, Iran

[2] Department of Tissue Engineering, School of Advanced Technologies in Medicine, Fasa University of Medical Sciences, Fasa, Iran

[3] Students' Scientific Research Center, Tehran University of Medical Sciences, Tehran, Iran

[4] Department of Endodontics, School of Dentistry, Tehran University of Medical Sciences, Tehran, Iran

[5] Department of Endodontics, School of Dentistry, Bahçeşehir University, Istanbul, Turkey

[6] Department of Microbiology, School of Medicine, Fasa University of Medical Sciences, Fasa, Iran

[7] Department of Obstetrics and Gynecology, Ziaeian Hospital, Tehran University of Medical Sciences, Tehran, Iran

Graphical Abstract

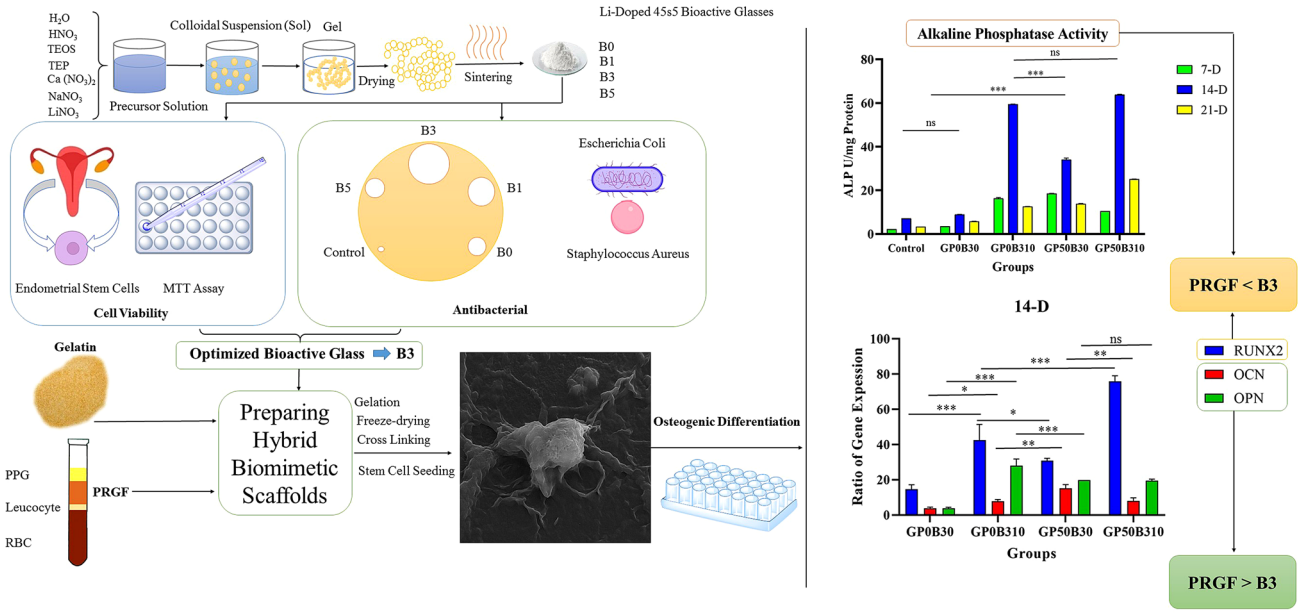

Keywords Bone regeneration · PRGF · Bioactive glass · Lithium · Antibacterial · Endometrial stem cell

Introduction

Bone is the primary tissue in the skeletal organ, whose essential functions include mobility, protection of other organs, and ion storage. Due to its fragile nature, it is highly vulnerable to damage, and it has a spontaneous repair just in minor defects. However, in defects with more than the critical size common in traumas and accidents, this repair does not happen spontaneously and has created many challenges for patients and orthopedic surgeons [1–4]. The incidence of osteoporosis has also increased the need for bone regeneration [5]. Tissue engineering as a new method based on the use of growth factors, stem cells, and biomaterials as scaffolding has created new horizons for improving bone defects [6]. Stem cells with the ability to self-renewal, as well as high proliferation and differentiation, play the role of cell source to create target tissues such as bone. However, it should be noted that in some cases, stem cells are also involved as the primary source of cancer, and some other pathological cases, such as endometriosis, may lead to infertility [7–10]. Meanwhile, mesenchymal stem cells, especially endometrial stem cells, have a high ability to proliferate, differentiate, and angiogenesis. Also, their harvesting method, unlike bone marrow stem cells, is not difficult or painful [11]. So, regarding the benefits mentioned above, endometrial stem cells attract significant attention in bone regeneration [12].

Moreover, another vital component of tissue engineering is growth factors. Growth factors are small molecules that play an essential role in cell proliferation and differentiation into target tissue [13, 14]. One of the most important sources is growth factors secreted by platelets. Hence, platelet concentrates such as platelet-rich plasma (PRP), platelet-rich fibrin (PRF), and plasma rich in growth factors (PRGF) have been widely used in tissue engineering, especially bone healing [15–18]. PRGF is a very small section of centrifuged blood containing Platelet-derived growth factors A and B (PDGF-A, PDGF-B), vascular endothelial growth factor (VEGF), BMP-2, transforming growth factor-beta (TGF-β), and insulin growth factor (IGF). These growth factors play a critical role in bone regeneration [19–21]. So, the application of PRGF in bone regeneration is increasing [22].

Furthermore, similarly to the natural tissues, stem cells need supportive materials for homing and delivering nutrients and growth factors. These materials should be biocompatible and have suitable interaction and affinity with cells, so they are called biomaterials [23]. Basically, biomaterials can be assumed as a temporary extracellular matrix for stem cells and play an essential role in proliferating, differentiating, and forming new tissue [24].Due to the predominantly mineral nature of bone tissue, ceramic biomaterials and especially bioactive glasses have been widely used in this field [25–29]. However, considering the organic phase of bone extracellular matrix (ECM), the application of biopolymers in bone regeneration is increasing [30, 31]. Hence,

organic–inorganic composites showed promising results in bone tissue engineering [32]. Amongst, gelatin has a great application in bone tissue engineering scaffolds due to its significant biocompatibility, cell adherence, low cost, and structural similarity to collagen as an organic phase of bone's ECM. So, gelatin-bioactive glasses are promising scaffolds in bone regeneration [33].

Also, one of the most important aspects of research is doping ions with better bone formation ability to their structure. According to the existing reports on the effects of lithium in improving cell proliferation, osteogenesis, and angiogenesis, doping this ion in bioactive glass seems to be an excellent strategy to improve its efficiency [34–38]. Many bone defects are also associated with traumas such as car accidents. It is common for high-energy traumas to result in open fractures that are challenging injuries and are associated with an increased risk of complications, like an infection [39]. There can be permanent functional loss or amputation from fracture-related infections (FRIs). Additionally, open flaps can cause sepsis as a serious life-threatening consequence in severe cases [40, 41]. Also, infections can deteriorate the bone healing process and delay it. Therefore, it is essential for scaffolds used for bone regeneration to be antibacterial [42]. Moreover, with the emerging COVID-19 pandemic and its significant effects on human life, the importance of antibacterial and antiviral materials has increased, and due to the antiviral and antibacterial properties of lithium, its addition to the biomaterial structure can improve its application [43–53].

So, it seems that scaffolds based on gelatin/PRGF/lithium-doped bioactive glasses seeded by endometrial cells can be considered a suitable approach for bone tissue engineering. In this study, first, 45s5 bioactive glass nanoparticles containing lithium with amounts of 1, 3, and 5% wt were prepared by the sol–gel method. Then, its optimal amount was determined based on its cell cytotoxicity and antibacterial properties. Then gelatin scaffolds Containing bioactive glass with the optimal amount of lithium and PRGF were prepared, and their ability to induce bone differentiation in endometrial stem cells was investigated. In addition, the effect of adding bioactive glass as well as PRGF on the mechanical properties of scaffolds was investigated.

Materials and Methods

Preparation of Li-Doped Bioactive Glass Nanoparticles

The sol–gel method has been used to synthesize bioactive glass particles [54, 55]. Briefly, based on 10 g bioactive glass 0.5 ml of nitric acid (HNO_3 65% MERK) was first added to 19.5 ml of distilled water (H_2O) and stirred for 10 min. Then 16.7 ml of tetraethyl orthosilicate (TEOS, Si $(OC_2H_5)_4$, Merck) was added to the acidic solution and stirred for acid hydrolysis for one hour. Following 1.5 mL of three ethyl phosphate (TEP, $(C_2H_5)_3PO_4$ Merck) is added to the material and left to stir for 25 min. Afterward, with a time interval of 20 min for each component, 10.5 g calcium nitrate (Ca $(NO_3)_2$, MERK), (6.72 g, 6.45 g, 5.9 g, 5.35 g) of sodium nitrate ($NaNO_3$, MERK), and (0 g, 0.46 g, 1.38 g, 2.31 g) of lithium nitrate ($LiNO_3$, MERK) are added, respectively. Lithium nitrate, used with 0, 1, 3, and 5 wt%, substitutes the sodium nitrates. Then whole material was stirred for one hour and stored at room temperature for 96 h. After 96 h, the obtained gel was first placed in the oven for 24 h at 70 °C and then kept at 120 °C for 48 h. The obtained precursor was ground by a hand mill. Subsequently, it is heated by the ratio of 10 °C/min and sintered at 750 °C to degrade alkoxides and remove nitrates. Bioactive glasses prepared with weight percentages of 0, 1, 3, and 5% Li_2O in their structures are named B0, B1, B3, and B5, respectively (Table 1).

Preparation of Hybrid Scaffolding

In this study, scaffolds were prepared by the freeze-drying method [56]. In preparing hybrid scaffolds, human-based PRGF was purchased from Noavaran Andish Pajoh. Briefly, they reported that collected blood from healthy volunteers poured into sterile test tubes having anticoagulants including 0.4 mL of 3.8% sodium citrate ($Na_3C_6H_5O_7$, MERK). Then tubes were centrifuged at 1400 rpm for 8 min. tubes now consist of three distinguished regions; red blood cells were precipitated at the bottom of the tube. A thin layer of leucocytes is located above red blood cells. The plasma region is above the leucocytes' layer. However, plasma region is divided into two regions. The first 0.5 ml upper of the leucocytes' layer is collected as PRGF; the rest was nominated as plasma poor in growth factors (PPGF). Subsequently, to activate PRGF, 50 µl of 10% calcium chloride ($CaCl_2$ MERK) was poured into PRGF, and after 15 min, the final product was achieved [57–61].

In order to find the optimal amount of gelatin, first solutions containing 5, 7.5, and 10% wt of gelatin were prepared and freeze-dried, then based on the obtained morphology, 5% was selected as the optimal amount for constructing

Table 1 Compositions of synthesized bioactive glass nanoparticles

Sample code	Components (%wt)				
	SiO_2	CaO	Na_2O	Li_2O	P_2O_5
B0	45	24.5	24.5	0	6.0
B1	45	24.5	23.5	1	6.0
B3	45	24.5	21.5	3	6.0
B5	45	24.5	19.5	5	6.0

hybrid scaffolds. So, an aqueous gelatin (Merck, microbiology grade, catalog number 104,070) solution was prepared at 25 °C. PRGF with the ratios (1: 1 and 3: 1 Gelatin: PRGF ratio wt/wt) and added to the gelatin solution and stirred for 10 min. Then the B3 (0, 5, 10, and 20% w/w) is added to the gelatin solution and stirred for 1.5 h. Following the mixture was molded and kept at 2 °C overnight to gel. Afterward, the molded materials were frozen at − 20 °C and − 80 °C for 48 h and 24 h, respectively. Subsequently, nanocomposites were lyophilized for 48 h at − 50 °C in a freezer dryer to obtain porous nanocomposites. The samples were then immersed in a solution of 0.5% glutaraldehyde in ethanol (%volume/volume) for 24 h to cross-link [62]. The samples were then washed with pure ethanol and immersed in distilled water to remove excess glutaraldehyde. Table 2 shows the sample code and their combinations.

Physical, Chemical, and Structural Properties of Scaffolds

By scanning electron microscopy (SEM, TESCAN-Vega3), we explored the morphology of bioactive glasses and scaffolds. Also measured the crystals with X-ray diffraction using a copper anode and a deflector at 40 kV and 2θ between 0° and 120°. Bioactivity was measured by immersing 10 mg of each bioactive glass in simulated body fluid (SBF) for seven days at 37 °C. Apatite on the samples was determined by X-ray diffraction after they had been washed with deionized water. We calculated the scaffold's porosity using Archimedes' law:

$$\text{Percentage of porosity} = (M2 - M3 - Md)/(M1 - M3) \times 100.$$

M1 refers to the weight of the container filled with alcohol, M2 refers to the container filled with alcohol after the scaffold is suspended, and M3 refers to the weight of the container filled with alcohol after the scaffold is removed. The scaffold's weight in the air is Md. The scaffolds' mechanical properties were evaluated on the Santam machine with a rate of 1 mm/min and a load cell of N 100. Each test examined 5 cylindrical specimens measuring 9 mm in diameter and 20 mm in height. Modulus is calculated based on the slope from the linear region of the stress–strain curve, and the strength equivalent to the maximum stress carried by each scaffold. Using a Dynamic Mechanical Thermal Analysis (DMTA) device (DMTA-PL, Model: Polymer Laboratory), we tested scaffolds at 1 Hz in the compressive mood and a temperature range of 0–150 °C, to measure their T_g. Also, Using an Inductively Coupled Plasma Optical Emission Spectrometry device (Varian-ES-730), we investigated the chemical composition of bioactive glass. Using the acid digestion approach, samples were processed by dissolving 100 mg of each bioactive glass in a digestion media made of 6 ml of HCl (ACS 37%, MERCK), 2 ml of HNO_3 (65%, MERCK), and 0.5 mL of HF (38–40%, MERCK). Then, 5 ml of 99.5% MERCK H_3BO_3 was added to the acid mixture. Since silica cannot be quantified because it generates volatile compounds (such as H_2SiF_6) in the presence of HF, its content could not be measured and was calculated by adding 100% to the measured value [63–66].

Table 2 Compositions of prepared scaffolds

Sample code	Components weight ratio			
	B0	B3	Gelatin	PRGF
GP0B30	0	0	1	0
GP25B30	0	0	1.5	0.5
GP50B30	0	0	1	1
GP0B35	0	0.05	0.95	0
GP0B310	0	0.10	0.90	0
GP0B010	0.10	0	0.90	0
GP0B320	0	0.20	0.80	0
GP50B35	0	0.05	0. 95	1
GP50B310	0	0.10	0.90	1
GP50B320	0	0.20	0.80	1

Biological Characterization

Antibacterial Properties

The sink method was used to evaluate the antibacterial properties of bioactive glass. Briefly, one gram of bioactive glass was first mixed with 1 ml of distilled water. The resulting extract was then diluted twice with distilled water to reach the concentration of 100 mg/ml. Then EMB culture medium was prepared for Gram-negative bacteria (ATCC 9637 *Escherichia coli*) and a Blood Agar culture medium for Gram-positive bacteria (Staphylococcus aureus ATCC 23235) was prepared. Using sterile swabs, the bacteria were removed from the suspensions prepared and cultured on the culture medium. The number of concentrations prepared from the extract plus one was created as a negative control well using a sterile pipette. 200 µl of each concentration was added to each well, and the only solvent was added to the negative control well. The media were then incubated in the incubator for 48 h. Finally, the zone of inhibitions was measured and reported.

Cell Adhesion

In this study, we used human endometrial stem cells obtained from the National Center for Genetic Resources of Iran (IBRC C1120). The morphology of the cells cultured on the scaffold was examined by SEM. In summary, human endometrial stem cells were cultured in 12 DMEM/F

(Gibco) medium supplemented with 10% FBS, 50 units/ml penicillin, 50 units/ml streptomycin, 5% CO_2, and the medium changed every day. Cells were then trypsinized to create a suspension of individual cells. The scaffolds were previously immersed in 70% ethanol, washed with PBS, and exposed to ultraviolet (UV) radiation overnight before the 3D culture of cells. 96 h after placing the suspension on the scaffold, the cells were fixed. For 1 h, the samples were immersed in 2.5% glutaraldehyde solution (Merck). The dehydration process uses alcohol with percentages of 10, 30, 70, 90, and 100%. Finally, the scaffolds were dried under the hood, exposed to dry air, and then covered with gold for vacuum SEM testing.

Cell Viability

We evaluated the cellular compatibility of synthesized bioactive glass and scaffolds containing them 1, 3, and 5 days after culture using the Calorimetric Method of 3-(4,5-dimethylthiazole-2-yl)-2,5-diphenyltetrazolium Bromide (MTT). Bioglass extract (10 mg/ml) was added to cells, or scaffolds were used to culture the cells. So, 4×10^4 cells were placed on each scaffold and incubated at 37 °C and 5% CO_2. Incubation was conducted for four hours with 200 µl of MTT solution at each interval. The crystals are then dissolved in the dimethyl sulfoxide (Merck) after removing the culture medium. Using the Expert 96 microplate reader (Asys Hitch, Ec Austria), we determined the amount of light absorption at 570 nm.

Investigation of Gene Expression

Following 14 and 21 days of induction of endometrial stem cells with osteogenic media on two-dimensional and three-dimensional tissue culture plates, qRT-PCR was used to measure the levels of Runx2, osteocalcin (OC), and osteopontin (OP) in the cultures. RNeasy Plus Mini Kit (Qiagen) was used for RNA extraction, and Easy cDNA Synthesis Kit (Cat.No.A101161) was used for complementary DNA synthesis. Real-time PCR analysis was performed to determine relative gene expression. In each PCR, 13 Power SYBRH Green PCR Master Mix (ABI PRISM, 4368702) was mixed with 12 ng cDNA and specific primers in a total volume of 20 µl. Table 3 lists the primer sequences designed and the temperatures for every gene observed during this reaction. In order to analyze the relative gene expression, we used the comparative method of Ct, $2^{-\Delta\Delta Ct}$ C_t. C_t values from the target genes were normalized to β-2-microglobulin (B2M) and calibrated with undifferentiated hEnSCs. A minimum of three independent experiments were conducted in each experiment, and the tests were repeated with the RiaGene6000 Qiagen.

Alkaline Phosphatase Activity

ALP activity was determined by converting p-nitrophenyl phosphate to p-nitrophenol and phosphate on days 7, 14, and 21 using a commercial kinetics kit (Pars Azmoun, Iran). A spectrophotometer measured the absorption change at 405 nm at 37 °C. For statistical analysis, all tests were repeated three times ($n = 3$), and SPSS software was used. A *t*-test was used to determine whether there was a significant difference between groups. A *p*-value of less than 0.05 was considered significant.

Table 3 Primers used in qRT-PCR

B2M	NM_004048.4	Homo sapiens beta-2-microglobulin (B2M)		
Forward primer	CCACTGAAAAAGATGAGTATGCCT		126 bp	60 °C
Reverse primer	CCAATCCAAATGCGGCATCTTCA			
RUNX2	NM_001278478.2	Homo sapiens RUNX family transcription factor 2 (RUNX2)		
Forward primer	TAGGCGCATTTCAGGTGCTT		105BP	60 °C
Reverse primer	TGCATTCGTGGGTTGGAGA			
Osteocalcin OC	NM_199173.6	Homo sapiens bone gamma-carboxyglutamate protein (BGLAP)		
Forward primer	CCTCACACTCCTCGCCCTATT		250 bp	60 °C
Reverse primer	GGTCAGCCAACTCGTCACA			
Osteopontin OP	NM_000582.3	Homo sapiens secreted phosphoprotein 1 (SPP1)		
Forward primer	GCCGAGGTGATAGTGTGGTT		149 bp	60 °C
Reverse primer	AACGGGGATGGCCTTGTATG			

Statistical Analysis

SPSS software was used for statistical analysis. Statistical differences between groups were assessed by analytical comparisons and analysis of variance. Statistical significance was considered in probability values of $p < 0.05$.

Results

Inductively Coupled Plasma Optical Emission Spectrometry (ICP-OES)

The presence and homogeneous distribution of all expected elements in the structure of bioactive glass, which includes Si, Na, P, Ca, and Li, is given in Table 4. The resulting mass results are the result of ICP-OES measurements, which show a relatively good agreement between the compositions of all prepared bioactive glass and the designed bioactive glass.

X-Ray Diffraction Analysis (XRD)

The XRD spectra before and after immersion of bioactive glasses in SBF are shown in Fig. 1. The wide peaks in (Fig. 1a and b) indicate the amorphous structure of the synthesized glass prior to SBF exposure. The appearance of peaks at $2\theta = 25.8°$ and $2\theta = 31.89°$ indicates the formation of crystalline hydroxyapatite (HCA) on the surface of the bioactive glass after seven days of immersion in SBF. However, with the increasing amount of lithium in the structure of bioactive glass, the intensity of peaks has decreased.

Antibacterial Properties

The antibacterial activity of bioglasses with different percentages of Li_2O against *Escherichia coli* (gram-negative) and Staphylococcus aureus (gram-positive) as a zone of inhibition of bacterial growth is shown in Table 5. Examination of the growth inhibition zone of bacteria in both types shows an increase of the inhibitory zone up to 3% wt (B3) and then a decrease in 5% wt of Li_2O (B5) in the structure of bioactive glass. Therefore, B3 contains in terms of optimal antibacterial properties.

Morphology and Cell Attachment (SEM)

Examination of SEM images of glass synthesized before immersion in SBF shows that, firstly, in all four groups, the synthesized nanoparticles have a size below 100 nm (Fig. 1c–f). Secondly, by adding lithium to the structure of bioactive glass, first, the morphology of the grains containing nanoparticles changed from round to plate. So, in the B3 sample, a plate structure was observed. But again in the B5 sample, the morphology of grain returns to spherical. Also, microstructure images of pure gelatin scaffolds in which prepared by solving 5, 7.5, and 10% wt/v of gelatin in water showed that scaffolds prepared with 5% wt of gelatin, have homogeneous pore size, higher porosity, and better interconnectivity (Fig. 2a–c). Moreover, the examination of the cell adhesion of scaffolds by SEM revealed the proper adhesion of the cells on the scaffold. However, in the groups containing bioactive glass, or PRGF lonely, or in combining groups, more pseudopods protruded emerged. So, better cell adhesion can be observed (Fig. 2e–l).

Cell Viability (MTT Assay)

The effects of bioactive glass ion extracts containing different amounts of lithium at 24, 72, and 120 h on endometrial stem cell proliferation are shown in Fig. 3a. The cell survival of the control group during each period was higher than the experimental group. However, with increasing the amount of lithium in the structure of bioactive glass up to 3% wt (B3), cell survival is significantly increased but decreased in B5, which contains 5% wt. These observed trends are valid in all time intervals. Also, cytotoxicity has been reduced by increasing the time of exposure of cells to bioactive glass extracts. Therefore, in this study, considering the results of cytotoxicity and antibacterial properties, B3 was selected as the bioactive glass with the optimal amount of lithium. Hence, B3 was used to prepare nanocomposite hybrid scaffolds.

Also, the cell viability results of gelatin/PRGF/lithium-doped bioactive glass scaffolds at similar time intervals are shown in Fig. 3b. Similarly, it is observed here that the cell survival rate on all scaffolds and at all-time intervals is lower than in the control group. However, adding bioactive glass, or PRGF, led to a significant increase in cell viability

Table 4 Measured compositions of bioactive glass nanoparticles in wt% determined by ICP-OES

Sample code	Weight percentage of elements				
	Si	Ca	Na	P	Li
B0	44.2 ± 0.10	24.1 ± 0.08	24.8 ± 0.16	6.9 ± 0.23	0
B1	45.9 ± 0.15	24.6 ± 0.17	22.1 ± 0.25	6.3 ± 0.27	1.1 ± 0.09
B3	45.6 ± 0.07	23.7 ± 0.14	21.3 ± 0.31	6.2 ± 0.18	3.2 ± 0.22
B5	45.3 ± 0.2	23.1 ± 0.11	19.8 ± 0.23	7.1 ± 0.08	4.7 ± 0.10

compared to scaffolds of neat gelatin. Furthermore, samples containing 10% by weight of bioactive glass B3 have higher cell survival than samples containing 20% by weight of B3. Therefore, the optimal amount of B3 in the structure is 10% wt. moreover, the addition of PRGF has led to an increase in cell viability. Also, comparing the results of scaffolds containing 10% of bioactive glass B0 and B3 (GP0B010, and GP0B310) also indicates the positive effect of lithium on cell survival. Moreover, comparing the results of different groups shows the synergistic effect of lithium-ion and PRGF in the scaffold in improving the survival of endometrial stem cells cultured on the scaffolds (especially in GP50B310).

Alkaline Phosphatase Activity

Measured values of alkaline phosphatase activity on days 7, 14, and 21 of endometrial stem cells cultured on scaffolds have been presented in Fig. 4. On all days, the volume of ALP production (ALP activity) in hybrid nanocomposite scaffolds, or scaffolds containing PRGF or bioactive glass lonely, significantly was higher than the control group and neat gelatin group. Also, alkaline phosphatase in all groups increased significantly from day 7 to day 14 and decreased significantly on day 21 compared to day 14. Moreover, an accurate investigation of the diagram shows that bioactive glass had a more effect on increasing ALP activity than PRGF.

Gene Expression Analysis (qRT-PCR)

qRT-PCR was utilized on days 14 and 21 to assess the expression of osteoblast markers, including Runx2, osteocalcin (OC), and osteopontin (OP) (Fig. 5). An evaluation of the acquired data reveals a considerable increase in Runx2 on day 14, followed by a drop on day 21 in scaffolds containing Li-doped bioactive glass. In addition, a comparison of the effects of Li-doped bioactive glass and PRGF on Runx2 expression reveals a statistically significant difference and a larger effect of bioactive glass in increasing the expression level of Runx2. Moreover, osteocalcin (OC) and osteopontin (OP) expression levels on day 21 were higher than on day 14. Comparatively, a closer examination reveals that PRGF was more successful at boosting osteocalcin (OC) and osteopontin (OP) levels than Li-doped bioactive.

Mechanical Properties and T_g Measurements

The results related to the measurement of compressive properties and glass transition temperature of scaffolds, as well as their porosity, are given in Table 6. The results show a significant increase in modulus with an increasing amount of bioactive glass. However, only increasing the amount of bioactive glass up to 10% wt has increased the strength, but the sample containing 20% wt of bioactive glass has decreased. Also, there is no discernible trend in the strain at break. In addition, the glass transition temperature increased slightly as the amount of bioactive glass in the structure increased. However, the presence of PRGF did not affect the mechanical properties and T_g of the samples.

Discussion

More than 200 million individuals worldwide have osteoporosis, a disease characterized by a reduction in bone mineral density. The main factors that induce bone deterioration in the world are obesity, genetic disorders, accidents, and aging [67]. Despite being the gold standard in treating bone lesions, autografts are not always used because of limitations, shortage of access, and mortality rates. Immune response and disease transmission are also stimulated by allografts [68, 69]. Hence, novel treatment approaches including tissue engineering, find emerging applications in bone repair. Tissue engineering research focuses on building scaffolds to support bone cells and encouraging and differentiating osteoblasts to regenerate bone. From a histological standpoint, bone tissue is a natural combination of bioceramic and polymer phases, principally apatite and collagen [70]. Therefore, nanocomposite polymer hybrid scaffolds have tremendous potential for bone tissue engineering [71, 72]. Porous 3D polymeric Nanocomposite scaffolds have been repeatedly reported to provide a suitable matrix for connecting and expanding different cell types [73]. In this group of scaffolds, gelatin stands out polymer because of its high cell adherence, low cost, and good blending abilities [31, 74]. Also, bioactive glasses are bioactive inorganic biomaterials that have been widely studied. These glasses are highly bioactive and have the capability that bonds with hard and soft tissues [75]. Gelatin/bioactive glass nanocomposites are usually bioresorbable scaffolds. Reviewing the in vitro degradation data of gelatin/bioactive glasses nanocomposites with different bioactive glasses showed that about 30% of the scaffolds' mass is resorbed at least 2 weeks after being put in SBF [76, 77]. Furthermore, in an in vivo study, little degradation was observed two weeks after implantation. The degradation time, however, correlated well with the regeneration time of new bone [78]. Releasing alkaline ions (like Ca^{2+} and Na^{+}) from bioactive glass and letting them dissolve neutralizes acidic byproducts of polymer degradation and slows down autocatalytic degradation [79]. The degradation times of lithium-doped bioactive glass nanocomposites may be slightly longer due to the densification of bioactive glass by lithium. Lithium doping in bioactive glass stimulates bone growth and inhibits its resorption, also giving it antibacterial properties [80].

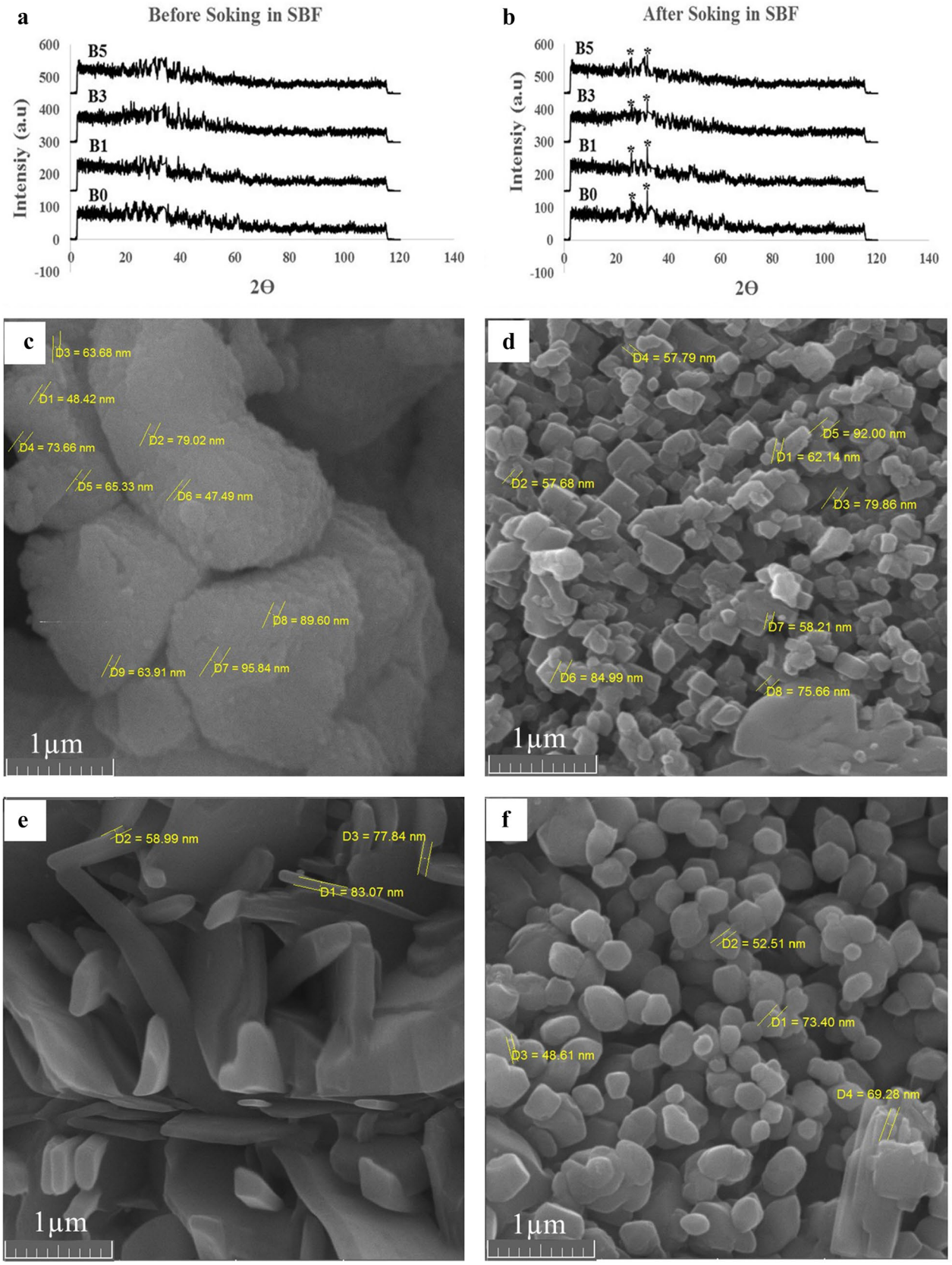
a
Before Soking in SBF
B5
B3
B1
B0
Intensiy (a.u)
2Θ
b
After Soking in SBF
B5
B3
B1
B0
Intensiy (a.u)
2Θ
c
D3 = 63.68 nm
D1 = 48.42 nm
D4 = 73.66 nm
D2 = 79.02 nm
D5 = 65.33 nm
D6 = 47.49 nm
D8 = 89.60 nm
D9 = 63.91 nm
D7 = 95.84 nm
1μm
d
D4 = 57.79 nm
D5 = 92.00 nm
D1 = 62.14 nm
D2 = 57.68 nm
D3 = 79.86 nm
D7 = 58.21 nm
D6 = 84.99 nm
D8 = 75.66 nm
1μm
e
D2 = 58.99 nm
D3 = 77.84 nm
D1 = 83.07 nm
1μm
f
D2 = 52.51 nm
D1 = 73.40 nm
D3 = 48.61 nm
D4 = 69.28 nm
1μm

◂**Fig. 1** XRD patterns, and SEM images of bioactive glasses. XRD patterns of the Li-doped bioactive glasses before (**a**) and after (**b**) immersion in SBF for 7 days (7D). The marked crystalline peaks in (**b**) indicate HCA. SEM images of bioactive glasses before immersion in SBF, **c** B0, **d** B1, **e** B3, **f** B5. Changes in grains morphology by adding lithium to their structure can be seen obviously

Also, growth factors have also been shown to be crucial in the healing procedure of damaged tissues. Since platelet-derived extracts, especially plasma rich in growth factors (PRGF), are good sources of them. Therefore, in this work, PRGF has also been used in the scaffolding structure [58]. The main novelty of the present study is that we induced promising osteogenic differentiation in endometrial stem cells by combining PRGF's growth factors and lithium simultaneously. This research also compares the effectiveness of each component on each osteogenic biomarker. Bioactive glass has been synthesized using the sol–gel method in this research. Since this approach produces nanostructured bioactive glass [81]. The good compliance of ICP results with the designed formulations (Table 4) can indicate that the sol–gel method was a suitable method for their synthesis. These results may be due to the differing sizes and electrical charge densities of sodium and lithium ions when replaced in the bioactive glass structure. Li-doped bioactive glasses have also shown densification caused by this change [82].

The amorphous structure of bioactive glasses has been proved in their XRD spectra before exposure to SBF (Fig. 1a). Additionally, the presence of characteristic HCA peaks ($2\theta = 25.8°$ and $2\theta = 31.89°$) after seven days of immersion in SBF may indicate that the synthesized glass is bioactive, and the reduction of HCA-related peaks may reflect the compactness of the structure of the bioglass due to the presence of lithium (Fig. 1b).

Antibacterial results and cell viability evaluation of bioactive glass B0, B1, B3, and B5 show that the presence of lithium-ion in the structure of bioactive glass (up to 3% wt) is beneficial against both Staphylococcus aureus (gram-positive) and *Escherichia coli* (gram-negative) bacteria as well as cell survival (Table 5 and Fig. 3a). As far as mentioned above, High-energy traumas may cause open fractures that may lead to fracture-related infections (FRI) [40, 41]. Also, it has been reported that the vast majority of the cases of bone infections are due to different types of Staphylococcus aureus as a gram-positive bacteria [83, 84]. Moreover, amongst gram negatives, *Escherichia coli* can cause bone infection [85, 86]. Both of them are considered to cause hospital-acquired infections and can cause osteomyelitis [87–90]. So, B3, and its composites can be assumed as suitable choices for bone regeneration especially in open flaps. Hence, its antibacterial function against hospital-acquired infections can improve its potential clinical application [91, 92].

Chemical-potential changes and pH changes lead to ion-channels function variations in bacteria and endometrial stem cells. These changes may have caused the aforementioned trend [37]. Other researchers have established that the ideal concentration of lithium in bioactive glass for antibacterial activities and cell survival is in the range of 2.5–5% wt. Therefore, there is a good agreement between the results of this research and their results [35, 93]. Accordingly, in this study, B3 (as the optimized bioglass) was used to prepare hybrid scaffolds. In this study, sponge scaffolds were prepared by freeze-drying. The appropriate size and regularity of cavities, as well as their interconnectivity, are crucial parameters for preparing scaffolds [94]. According to the above criteria, 5% wt of gelatin was the optimal amount for making scaffolds. Comparing the size of the cavities of the synthesized scaffolds (near to 200 µm) with bone and stem cells (less than 20 µm) demonstrates the appropriate size of the formed scaffolds for cell homing. Additionally, SEM images of cell adhesion to scaffolds also demonstrated proper adhesion. Images showed that bioactive glass improved cell adhesion which may be due to the interaction between the HCA layer created by the bioglass and cell surface proteins, such as fibronectin and vitronectin. Cell adhesion is also affected by calcium, silicon, and lithium ions, especially calcium ions [95–100]. Furthermore, increasing the scaffold structure's modulus due to bioactive glass's presence may improve cell adhesion [101].

Also, scaffolds containing PRGF showed better cell adhesion, possibly because of playing a crucial role of growth factors in the structure of PRGF, especially platelet-derived growth factors (Fig. 2e–l) [12, 70]. Other researchers have confirmed these findings [102, 103]. There is much interest today in using PRGF for bone repair in dentistry applications [104].

MTT results confirm this trend in cell adhesion. Also, reduced cell survival in scaffolds relative to controls may be attributed to the very small amount of residual glutaraldehyde in scaffolds structure or high ions concentrations of bioglasses [105, 106].

It has also been observed that cell viability depends on peripheral ions, especially lithium-ion, and samples with 20% wt of bioactive glass have a lower survival rate than samples with 10% wt. However, lithium increases cell survival throughout the all-time intervals, a trend that can be attributed to the activation of the wnt signaling pathways and the wnt/β-catenin signaling pathway [107]. In addition, the increase in cell survival rate with PRGF in the structure can also be attributed to the presence of TGF- β, PDGF, and IGF [108, 109].

The primary marker of osteoblasts, alkaline phosphatase, is a membrane enzyme that hydrolyzes phosphate ions, allowing the formation of hydroxyapatite crystals and stimulating mineralization. ALP plays a crucial role in bone

Table 5 Antibacterial properties of synthesized bioactive glass nanoparticles

Sample code	Zone of Inhibition (mm)	
	Escherichia coli	Staphylococcus aureus
B0	12	11
B1	14	13
B3	18	16
B5	13	12

regeneration and differentiation [110]. Compared to pure gelatin scaffold, Li-doped bioactive glass, PRGF, and a combination group showed a substantial increase in ALP activity with increasing culture time. ALP plays a role in ECM maturation, and the presence of bioactive components in scaffolds can enhance its production and activity [111]. Cell differentiation, bone protein expression, and ALP synthesis are affected by bioactive glass nanoparticles. Furthermore, researchers describe bioactive glass nanoparticles as bone differentiation factors due to the high concentration of silicate ions in their composition [112]. However, the presence of lithium-ion is also very effective in improving bone differentiation and increasing ALP activity due to its proven effect in activating wnt and wnt/β-catenin signaling pathways [113–115]. Also, BMP-2, IGF, and TGF-β that are found in the PRGF in the scaffolds structure enhance the activity of ALP [116, 117]. Although, the results show that the role of bioactive glass in increasing ALP activity is more significant.

At 14 and 21 days, OC and OP proteins, and the transcription factor Runx2, which are primary biomarkers of bone formation, were examined. Osteocalcin is the primary non-collagenous protein, which is formed 1–2% of the total content of matrix proteins. It promotes mineralization and is commonly expressed in calcified bone and cartilage, whereas

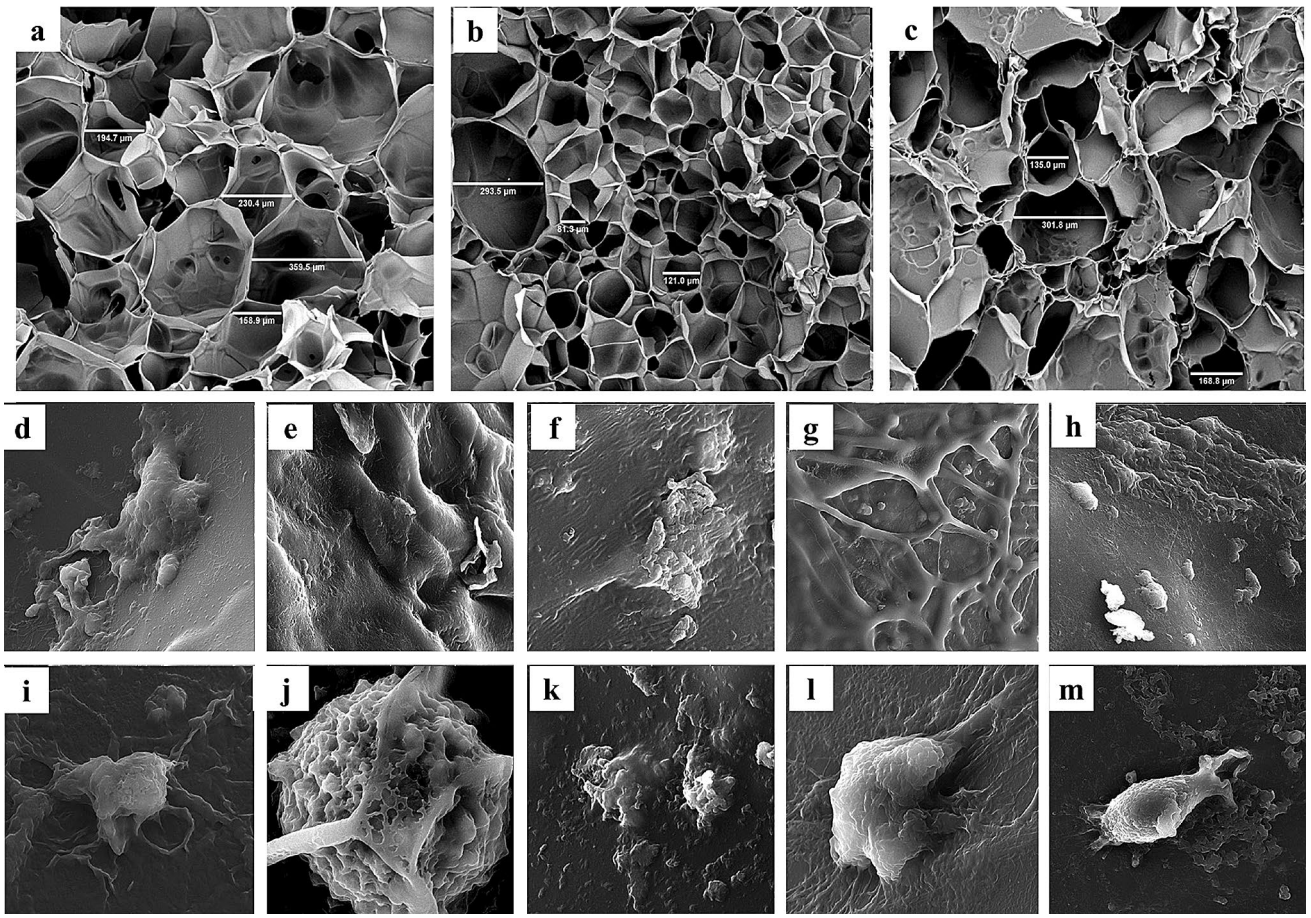

Fig. 2 SEM images of neat gelatin scaffolds prepared by different content of gelatin, and human endometrial stem cells (hEnSCs) attachment on scaffolds. SEM images of neat gelatin scaffolds containing **a** 5% wt/v, **b** 7.5% wt/v and **c** 10% wt/v of gelatin in water. Regularity and interconnectivity is higher in (**a**). Stem cells have shown good attachment on scaffolds, especially those containing bioactive glass and PRGF or both of them. **d** GP0B30, **e** GP0B35, **f** GP0B310, **g** GP0B320, **h** GP50B30, **i** GP50B35, **j** GP50B310, **k** GP50B320, **l** GP25B30, **m** GP0B010

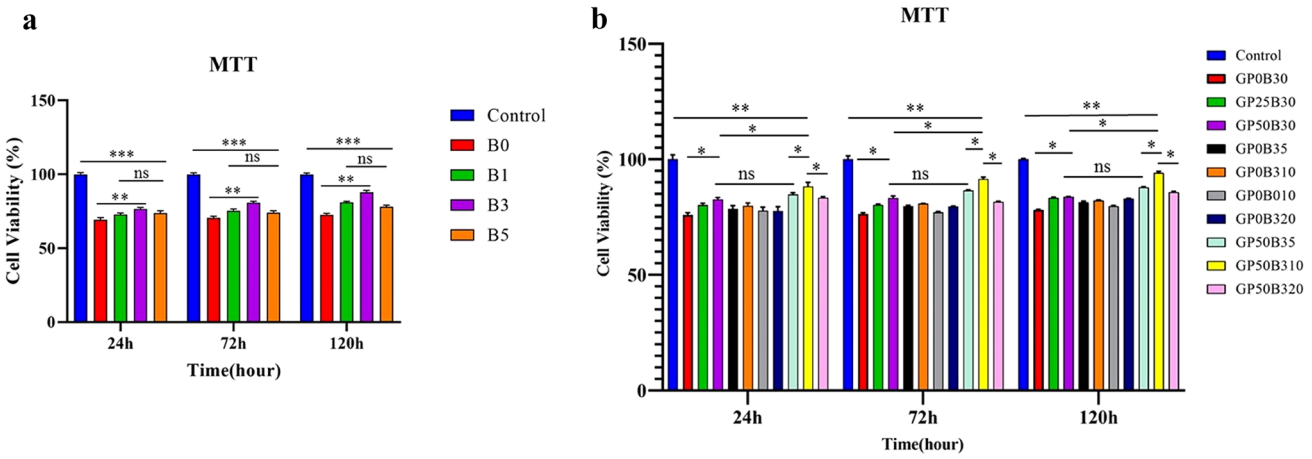

Fig. 3 Cell viability (MTT) results of bioactive glasses and scaffolds in 24, 72, and 120 h. **a** B3 shows higher cell viability comparing other bioglasses in all time intervals. **b** Cell viability significantly is higher in GP50B310 than all other scaffolds (p-value = p, $^{*}p < 0.05$, $^{**}p < 0.01$, $^{***}p < 0.001$)

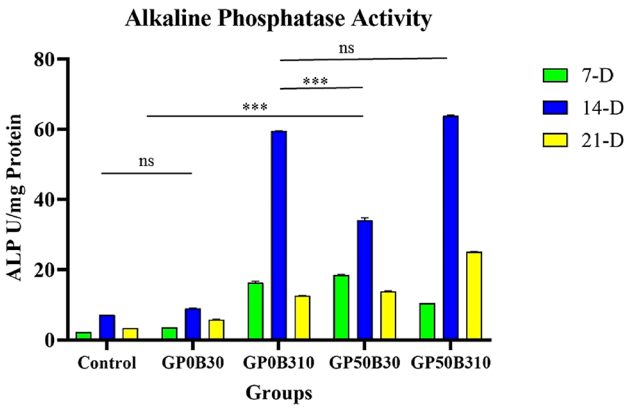

Fig. 4 ALP activity of results in 7, 14, and 21 Days. Li-doped bioglass, and PRGF both increase ALP activity. Although bioactive glass is more effective in increasing ALP activity (p-value = p, $^{*}p < 0.05$, $^{**}p < 0.01$, $^{***}p < 0.001$)

Runx2 is a major transcription factor for osteoblast differentiation [20, 118, 119]. Osteogenesis is committed by multiple cytokines, hormones, and signaling cascades e.g. wnt and β-catenin [120, 121]. In particular, Runx2 plays a critical role in osteoblast differentiation by expressing osteoblastogenic markers like ALP, OC, and OP [122]. Runx2 is also known to modulate the transcription of mineralizing genes [123]. Runx2 has been shown to have a vital role to convert human fibroblasts into functional osteoblasts [124]. Various stimuli can also affect Runx2 post-translationally through phosphorylation, ubiquitination, and acetylation [125]. The level of Runx2 rises when osteoblasts are immature and decrease when they mature. In osteoblast maturation, its down-regulation may be beneficial [126]. By expressing transcription factors and bone matrix proteins, Runx2 has an autoregulatory mechanism [127]. Indeed, Runx2 controlled

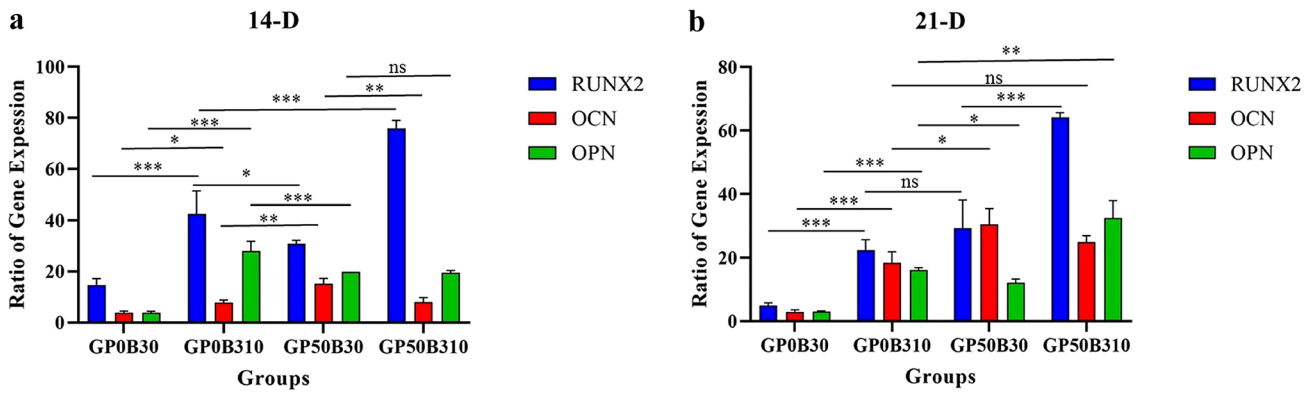

Fig. 5 Gen expression of results in 14, and 21 Days. Li-doped bioglass increased Runx2 drastically, but PRGF is more effective in increasing OC, and OP expression (p-value = p, $^{*}p < 0.05$, $^{**}p < 0.01$, $^{***}p < 0.001$)

Table 6 Mechanical properties, T_g, and porosity of scaffolds

Sample code	Mechanical properties			T_g (°C)	Porosity (%)
	Strength (MPa)	Modulus (MPa)	Max. strain (%)		
GP0B30	1.34 ± 0.17	5.11 ± 0.23	40.17 ± 12.31	61.8	96.4 ± 1.3
GP50B30	1.35 ± 0.22	4.97 ± 0.28	26.25 ± 3.2	60.7	96.5 ± 1.7
GP0B35	1.94 ± 0.27	11.43 ± 0.45	27.45 ± 3.37	63.4	94.1 ± 0.8
GP0B310	2.69 ± 0.4	18.17 ± 0.38	18.88 ± 4.81	67.3	92.6 ± 1.2
GP50B310	2.64 ± 0.38	18.19 ± 0.58	26.16 ± 2.23	67.5	91.9 ± 0.5
GP0B320	2.61 ± 0.61	23.58 ± 0.87	12.61 ± 2.13	70.9	90.9 ± 0.6

ALP promoter activity, establishing a positive feedback loop between ALP and Runx2 that controlled osteoblast development [122]. Also, in this research, the similarity of trends in ALP-activity results and Runx2 expressions on day 14 and day 21 was observed. Therefore, these investigations help explain the trends in ALP activity and Runx2 that have been noticed.

Also, OP affects osteoblast, and osteocyte adhesion and differentiation [128]. For 21 days, mRNA expression increased in all experimental groups. It is important to note that both OC and OP proteins indicate mineralization potential. However, OP protein was more expressed in this study than OC protein. Also, the presence of lithium-containing bioactive glass also increased drastically in Runx2. This trend may be owing to the synergistic action of lithium-ion and other ions (particularly Si ion) in bioactive glass, as well as lithium's activation and boosting of the Wnt signaling pathway, which increases Runx2 expression [129–131]. Like ALP activity, bioactive glass nanoparticles and PRGF increased OC and OP protein expression. PRGF growth factors increased OP and OC expression higher than Li-doped bioactive glass. The autocrine effect of PRGF's growth factors may explain the observed trend [132]. OC and OP proteins and Runx-2 transcription factors were more abundant in the hybrid sample containing both bioactive components. Lithium can also stimulate stem cells to secrete exosomes, affecting tissue repair [133]. In addition, since blood plasma is one of the main sources of exosome extraction, it seems that one of the main factors affecting the improvement of bone regeneration in this research is the presence of exosomes in PRGF [134–139].

Differentiation towards a bone category is significantly affected by the modulus and stiffness of the scaffold. According to the mechanical properties test, the presence of bioactive glass leads to a continuous increase in modulus due to its stiffness over gelatin. It is found that their strength only increases up to 10% wt of bioactive glass. This can be attributed to a lack of homogeneity and agglomeration of bioactive glass in the structure of the resulting nanocomposites, leading to stress concentration and early failure of the samples. The fluctuation trend of strain at the breaking point is also related to failure mechanics due to compression and separation of small parts from the specimens during the compression process, which lead to stress concentration and early failure [140]. Increases in glass transition temperature with increasing amounts of bioactive glass can be explained by inhibiting the mobility of gelatin polymer chains by bioactive glass nanoparticles. PRGF has minimal effect on mechanical behavior and glass transition temperature due to the small amount of growth factor small molecules it contains compared to gelatin polymer. Furthermore, the decreased porosity of structures prepared with increased bioactive glass may also be attributed to the formation of wholly closed cavities in bioactive glass [56].

Conclusion

In this research, new hybrid nanocomposites based on gelatin/PRGF/Li-doped 45s5 bioactive glass nanoparticles were prepared by freeze-drying method. Characterization of the synthesized bioactive glass showed that adding 3% wt of lithium to the structure of the 45s5 bioactive glass prepared by the sol–gel method optimizes its biocompatibility and antibacterial properties. Also, interestingly, it was observed that lithium has antibacterial properties against both gram-positive and gram-negative bacteria. Also, the presence of bioactive glass and PRGF alone or in combination improves cell viability and cell adhesion. However, the optimal amount of bioactive glass in the scaffold structure is 10% wt, and cytotoxicity increases by 20% wt. Also, the synergistic effects of lithium ions and silicon ions can cause a significant increase in ALP activity and Runx-2 expression. While the growth factors in PRGF mainly increase the expression of OP and OC genes. In addition, the presence of bioactive glass increases the modulus and T_g of scaffolds. While the presence of growth factor had little effect on the mechanical properties and T_g. basically, it seems that the hybrid scaffold used was able to create the survival of endometrial stem cells and their adhesion to the surface and cause their osteogenic differentiation. Finally, a general review of the results of this study suggested that the strategy used in this study includes combining bioactive glass as a bone-inducing mineral phase, gelatin as a biocompatible polymer, PRGF as a source of

growth factor, and lithium-ion as a bone-inducing agent as well as an antibacterial agent can be considered as a good approach to repair bone lesions.

Author Contributions All authors contributed to the study's conception and design. Material preparation, data collection, and analysis were performed by ARF, JA, and SM. The first draft of the manuscript was written by ARF and other authors including MHN, SEB, MA, and SN reviewed the manuscript and commented on previous versions of the manuscript. All authors read and approved the final manuscript. Material preparation, data collection, and analysis were performed by ARF, JA, and SM. The first draft of the manuscript was written by ARF. MHN, SEB, MA, and SN reviewed the manuscript. ARF and SEB prepared Figs. 1, 2, 3, 4 and 5. SN and MA prepared Tables 1, 2, 3, 4 and 6.

Funding This work was supported by School of Advanced Technologies in Medicine, Tehran University of Medical Sciences (Grant Number 98-01-87-41020).

Declarations

Conflict of interest The authors have no relevant financial or non-financial interests to disclose.

References

1. Lopes D et al (2018) Bone physiology as inspiration for tissue regenerative therapies. Biomaterials 185:240–275
2. Oryan A, Monazzah S, Bigham-Sadegh A (2015) Bone injury and fracture healing biology. Biomed Environ Sci 28(1):57–71
3. Winkler T et al (2018) A review of biomaterials in bone defect healing, remaining shortcomings and future opportunities for bone tissue engineering: the unsolved challenge. Bone Joint Res 7(3):232–243
4. Riester O et al (2021) Challenges in bone tissue regeneration: stem cell therapy, biofunctionality and antimicrobial properties of novel materials and its evolution. Int J Mol Sci 22(1):192
5. Iñiguez-Ariza NM, Clarke BL (2015) Bone biology, signaling pathways, and therapeutic targets for osteoporosis. Maturitas 82(2):245–255
6. Tang G et al (2021) Recent trends in the development of bone regenerative biomaterials. Front Cell Dev Biol 9:15
7. Giannone G et al (2019) Endometrial cancer stem cells: role, characterization and therapeutic implications. Cancers 11(11):1820
8. Cousins FL, Gargett CE (2018) Endometrial stem/progenitor cells and their role in the pathogenesis of endometriosis. Best Pract Res Clin Obstet Gynaecol 50:27–38
9. Tanbo T, Fedorcsak P (2017) Endometriosis-associated infertility: aspects of pathophysiological mechanisms and treatment options. Acta Obstet Gynecol Scand 96(6):659–667
10. Mahdavinezhad F et al (2021) The potential relationship between different human female reproductive disorders and sperm quality in female genital tract. Reprod Sci 15:1–16
11. Alizadeh A et al (2016) Synthesis of calcium phosphate-zirconia scaffold and human endometrial adult stem cells for bone tissue engineering. Artif Cells Nanomed Biotechnol 44(1):66–73
12. Ai J et al (2017) BMP-2 can promote the osteogenic differentiation of human endometrial stem cells. Asian Biomed 8(1):21–29
13. Ren X et al (2020) Growth factor engineering strategies for regenerative medicine applications. Front Bioeng Biotechnol 7:469
14. Kuroda Y et al (2019) Clinical application of injectable growth factor for bone regeneration: a systematic review. Inflamm Regen 39(1):1–10
15. Badran Z et al (2018) Platelet concentrates for bone regeneration: current evidence and future challenges. Platelets 29(2):105–112
16. Fernandes G, Yang S (2016) Application of platelet-rich plasma with stem cells in bone and periodontal tissue engineering. Bone Res 4(1):1–21
17. Farmani AR et al (2021) Application of platelet rich fibrin in tissue engineering: focus on bone regeneration. Platelets 32(2):183–188
18. Solakoglu Ö et al (2020) The use of plasma rich in growth factors (PRGF) in guided tissue regeneration and guided bone regeneration: a review of histological, immunohistochemical, histomorphometrical, radiological and clinical results in humans. Ann Anat Anatomischer Anzeiger 231:151528
19. Nishiyama K et al (2016) Basic characteristics of plasma rich in growth factors (PRGF): blood cell components and biological effects. Clin Exp Dental Res 2(2):96–103
20. Anitua E et al (2016) Biological effects of plasma rich in growth factors (PRGF) on human endometrial fibroblasts. Eur J Obst Gynecol Reprod Biol 206:125–130
21. Huchim-Chablé M et al (2021) Calcium sulfate and plasma rich in growth factors enhance bone regeneration after extraction of the mandibular third molar: a proof of concept study. Materials 14(5):1126
22. Sheykhhasan M, Seifalian A (2021) Plasma-rich in growth factor and its clinical application. Curr Stem Cell Res Ther 16(6):730–744
23. Zhao X, Cui K, Li Z (2019) The role of biomaterials in stem cell-based regenerative medicine. Future Med Chem 11(14):1777–1790
24. Gaharwar AK, Singh I, Khademhosseini A (2020) Engineered biomaterials for in situ tissue regeneration. Nat Rev Mater 5(9):686–705
25. Ginebra M-P et al (2018) Bioceramics and bone healing. Effort Open Rev 3(5):173–183
26. Zafar MJ, Zhu D, Zhang Z (2019) 3D printing of bioceramics for bone tissue engineering. Materials 12(20):3361
27. Hench LL, Roki N, Fenn MB (2014) Bioactive glasses: Importance of structure and properties in bone regeneration. J Mol Struct 1073:24–30
28. Lalzawmliana V et al (2020) Mesoporous bioactive glasses for bone healing and biomolecules delivery. Mater Sci Eng C 106:110180
29. Jablonská E et al (2020) A review of in vitro cell culture testing methods for bioactive glasses and other biomaterials for hard tissue regeneration. J Mater Chem B 8(48):10941–10953
30. Guo L et al (2021) The role of natural polymers in bone tissue engineering. J Control Release 338:571–582
31. Filippi M et al (2020) Natural polymeric scaffolds in bone regeneration. Front Bioeng Biotechnol 8:15
32. Shao N et al (2018) Development of organic/inorganic compatible and sustainably bioactive composites for effective bone regeneration. Biomacromol 19(9):3637–3648
33. Sergi R, Bellucci D, Cannillo V (2020) A review of bioactive glass/natural polymer composites: state of the art. Materials 13(23):15
34. Schatkoski VM et al (2021) Current advances concerning the most cited metal ions doped bioceramics and silicate-based bioactive glasses for bone tissue engineering. Ceram Int 47(3):2999–3012

35. Miguez-Pacheco V et al (2016) Development and characterization of lithium-releasing silicate bioactive glasses and their scaffolds for bone repair. J Non-Cryst Solids 432:65–72
36. Zhang K et al (2019) A comparison of lithium-substituted phosphate and borate bioactive glasses for mineralised tissue repair. Dent Mater 35(6):919–927
37. da Silva JG et al (2017) Optimisation of lithium-substituted bioactive glasses to tailor cell response for hard tissue repair. J Mater Sci 52(15):8832–8844
38. Moghanian A et al (2018) A comparative study on the in vitro formation of hydroxyapatite, cytotoxicity and antibacterial activity of 58S bioactive glass substituted by Li and Sr. Mater Sci Eng C 91:349–360
39. Neubauer T, Bayer G, Wagner M (2006) Open fractures and infection. Acta Chir Orthop Traumatol Cech 73(5):301
40. Lu V et al (2022) Fracture related infections and their risk factors for treatment failure: a major trauma centre perspective. Diagnostics 12(5):1289
41. Zalavras CG (2017) Prevention of infection in open fractures. Infect Dis Clin 31(2):339–352
42. Rupp M, Popp D, Alt V (2020) Prevention of infection in open fractures: where are the pendulums now? Injury 51:S57–S63
43. Farmani AR et al (2021) Anti-IgE monoclonal antibodies as potential treatment in COVID-19. Immunopharmacol Immunotoxicol 15:1–6
44. Farmani AR et al (2021) An overview on tumor treating fields (TTFields) technology as a new potential subsidiary biophysical treatment for COVID-19. Drug Deliv Transl Res 24:1–11
45. Farmani AR et al (2021) Potential application of picosecond pulsed electric field (PPEF): advanced bioelectrical technology for potential COVID-19 treatment. J New Mater Electrochem Syst 24(4):293–296
46. Mahdavinezhad F et al (2022) COVID-19 and varicocele: the possible overlap factors and the common therapeutic approaches. Am J Reproduct Immunol. 37:13518
47. Huang X et al (2021) Antiviral Biomaterials. Matter 4:1892–1918
48. Kumari S, Chatterjee K (2021) Biomaterials-based formulations and surfaces to combat viral infectious diseases. APL Bioeng 5(1):011503
49. Murru A et al (2020) Lithium's antiviral effects: a potential drug for CoViD-19 disease? Int J Bipolar Disord 8:1–9
50. Spuch C et al (2020) Does lithium deserve a place in the treatment against COVID-19?: a preliminary observational study in six patients, case report. Front Pharmacol 11:1347
51. Liang C et al (2021) Antibacterial evaluation of lithium-loaded nanofibrous poly (L-lactic acid) membranes fabricated via an electrospinning strategy. Front Bioeng Biotechnol 9:334
52. Cordero HP et al (2021) Li-doped bioglass® 45S5 for potential treatment of prevalent oral diseases. J Dent 105:103575
53. Keikhosravani P et al (2021) Bioactivity and antibacterial behaviors of nanostructured lithium-doped hydroxyapatite for bone scaffold application. Int J Mol Sci 22(17):9214
54. Vafa E, Bazargan-Lari R, Bahrololoom ME (2021) Synthesis of 45S5 bioactive glass-ceramic using the sol-gel method, catalyzed by low concentration acetic acid extracted from homemade vinegar. J Market Res 10:1427–1436
55. Barabadi Z et al (2016) Fabrication of hydrogel based nanocomposite scaffold containing bioactive glass nanoparticles for myocardial tissue engineering. Mater Sci Eng C 69:1137–1146
56. Jalise SZ, Baheiraei N, Bagheri F (2018) The effects of strontium incorporation on a novel gelatin/bioactive glass bone graft: in vitro and in vivo characterization. Ceram Int 44(12):14217–14227
57. Brazdeikytė V, Baliutavičiūtė D, Rokicki JP (2021) Influence of PRGF and PRF on postextractive alveolus regeneration: a randomised controlled trial. Quintessence Int 2:1–8
58. Brucoli M et al (2018) Plasma rich in growth factors (PRGF) for the promotion of bone cell proliferation and tissue regeneration. Oral Maxillofac Surg 22(3):309–313
59. Batas L, Tsalikis L, Stavropoulos A (2019) PRGF as adjunct to DBB in maxillary sinus floor augmentation: histological results of a pilot split-mouth study. Int J Implant Dent 5(1):1–7
60. Ratiu C et al (2019) PRGF-modified collagen membranes for guided bone regeneration: spectroscopic, microscopic and nano-mechanical investigations. Appl Sci 9(5):1035
61. Anitua E et al (2022) Composite alginate-gelatin hydrogels incorporating PRGF enhance human dental pulp cell adhesion, chemotaxis and proliferation. Int J Pharm 617:121631
62. Nagiah N et al (2013) Electrospinning of poly (3-hydroxybutyric acid) and gelatin blended thin films: fabrication, characterization, and application in skin regeneration. Polym Bull 70(8):2337–2358
63. Kumar A et al (2017) Mesoporous 45S5 bioactive glass: synthesis, in vitro dissolution and biomineralization behavior. J Mater Chem B 5(44):8786–8798
64. Zheng K et al (2019) Toward highly dispersed mesoporous bioactive glass nanoparticles with high Cu concentration using Cu/ascorbic acid complex as precursor. Front Chem 7:497
65. Mutlu N et al (2022) Effect of Zn and Ga doping on bioactivity, degradation, and antibacterial properties of borate 1393–B3 bioactive glass. Ceram Int 48(11):16404–16417
66. Kurtuldu F et al (2021) Cerium and gallium containing mesoporous bioactive glass nanoparticles for bone regeneration: Bioactivity, biocompatibility and antibacterial activity. Mater Sci Eng C 124:112050
67. Hemmati E et al (2021) Prevalence of primary osteoporosis and low bone mass in postmenopausal women and related risk factors. J Educ Health Promot 10:204–204
68. Wang W, Yeung KWK (2017) Bone grafts and biomaterials substitutes for bone defect repair: a review. Bioact Mater 2(4):224–247
69. Baldwin P et al (2019) Autograft, allograft, and bone graft substitutes: clinical evidence and indications for use in the setting of orthopaedic trauma surgery. J Orthopaedic Trauma 33(4):203–213
70. Ansari M (2019) Bone tissue regeneration: biology, strategies and interface studies. Prog Biomater 8(4):223–237
71. Mondragón E et al (2020) Mimicking the organic and inorganic composition of anabolic bone enhances human mesenchymal stem cell osteoinduction and scaffold mechanical properties. Front Bioeng Biotechnol 8:753
72. Liu L et al (2020) Homogeneous organic/inorganic hybrid scaffolds with high osteoinductive activity for bone tissue engineering. Polym Testing 91:106798
73. Abbasi N et al (2020) Porous scaffolds for bone regeneration. J Sci 5(1):1–9
74. Kuo Z-K et al (2016) Osteogenic differentiation of preosteoblasts on a hemostatic gelatin sponge. Sci Rep 6(1):32884
75. Pantulap U, Arango-Ospina M, Boccaccini AR (2021) Bioactive glasses incorporating less-common ions to improve biological and physical properties. J Mater Sci 33(1):3
76. Huang G et al (2021) Gelatin/bioactive glass composite scaffold for promoting the migration and odontogenic differentiation of bone marrow mesenchymal stem cells. Polym Testing 93:106915
77. Abd El-Aziz AM et al (2021) Viscoelasticity, mechanical properties, and in vitro bioactivity of gelatin/borosilicate bioactive glass nanocomposite hydrogels as potential scaffolds for bone regeneration. Polymers 13(12):2014
78. Kazemi M et al (2018) Bone regeneration in rat using a gelatin/bioactive glass nanocomposite scaffold along with endothelial cells (HUVEC s). Int J Appl Ceram Technol 15(6):1427–1438

79. Dziadek M, Stodolak-Zych E, Cholewa-Kowalska K (2017) Biodegradable ceramic-polymer composites for biomedical applications: a review. Mater Sci Eng C 71:1175–1191
80. Durand LAH et al (2019) Lithium-containing bioactive glasses for bone regeneration. Biomed Ther Clin Appl Bioact Glasses 15:201–217
81. Zheng K, Boccaccini AR (2017) Sol-gel processing of bioactive glass nanoparticles: a review. Adv Coll Interface Sci 249:363–373
82. Khorami M et al (2011) In vitro bioactivity and biocompatibility of lithium substituted 45S5 bioglass. Mater Sci Eng C 31(7):1584–1592
83. Zambanini T et al (2019) Bioactive glasses for treatment of bone infections. biomedical, therapeutic and clinical applications of bioactive glasses. Elsevier, pp 383–415
84. Wang L, Ruan S (2017) Modeling nosocomial infections of methicillin-resistant staphylococcus aureus with environment contamination. Sci Rep 7(1):580
85. Lee J et al (2017) Emphysematous Osteomyelitis due to *Escherichia coli*. Infect Chemother 49(2):151–154
86. Luu T, Reid G, Lavery B (2022) *Escherichia coli* associated hematogenous sternoclavicular joint osteomyelitis: a rare condition with a rare causative pathogen. IDCases 27:e01381
87. Fukunaga BT et al (2016) Hospital-acquired methicillin-resistant staphylococcus aureus bacteremia related to medicare antibiotic prescriptions: a state-level analysis. Hawaii J Med Public Health 75(10):303–309
88. Hayajneh AA et al (2021) Predictors of growth of *Escherichia coli* on lab coats as part of hospital-acquired infection transmission through healthcare personnel attire. Int J Clin Pract 75(11):e14815
89. Yamashita T et al (2021) Reconstruction of *E. coli* osteomyelitis of costa: a case report. Plastic Reconstruct Surgery Global Open 9(2):e3413
90. Kavanagh N et al (2018) Staphylococcal osteomyelitis: disease progression, treatment challenges, and future directions. Clin Microbiol Rev 31(2):e00084
91. Lu H et al (2016) Biomaterials with antibacterial and osteoinductive properties to repair infected bone defects. Int J Mol Sci 17(3):334
92. Pahlevanzadeh F et al (2022) A review on antibacterial biomaterials in biomedical applications: from materials perspective to bioinks design. Polymers 14(11):2238
93. Moghanian A, Firoozi S, Tahriri M (2017) Synthesis and in vitro studies of sol-gel derived lithium substituted 58S bioactive glass. Ceram Int 43(15):12835–12843
94. Govindan R et al (2020) Effect of phosphate glass reinforcement on the mechanical and biological properties of freeze-dried gelatin composite scaffolds for bone tissue engineering applications. Mater Today Commun 22:100765
95. Zou S et al (2009) The effects of silicate ions on human osteoblast adhesion, proliferation, and differentiation. J Biomed Mater Res B 90B(1):123–130
96. Lu ZA et al (2011) The effect of extracellular calcium on cellular adhesion of mesenchymal stem cells to substrates. FASEB J 25(S1):6787–6787
97. Marchesano V et al (2015) Effects of lithium niobate polarization on cell adhesion and morphology. ACS Appl Mater Interfaces 7(32):18113–18119
98. Zhang Y et al (2019) The effect of amino-functionalized mesoporous bioactive glass on MC3T3-E1 cells in vitro stimulation. Compos B Eng 172:397–405
99. Nokhasteh S et al (2018) Effect of bioactive glass nanoparticles on biological properties of PLGA/collagen scaffold. Prog Biomater 7(2):111–119
100. Thamma U et al (2021) Nanostructure of bioactive glass affects bone cell attachment via protein restructuring upon adsorption. Sci Rep 11(1):5763
101. Wang Y-K, Chen CS (2013) Cell adhesion and mechanical stimulation in the regulation of mesenchymal stem cell differentiation. J Cell Mol Med 17(7):823–832
102. Wu C-L et al (2012) Platelet-rich fibrin increases cell attachment, proliferation and collagen-related protein expression of human osteoblasts. Aust Dent J 57(2):207–212
103. Charoensuk T et al (2016) In vitro bioactivity and stem cells attachment of three-dimensionally ordered macroporous bioactive glass incorporating iron oxides. J Non-Cryst Solids 452:62–73
104. Shirani G et al (2017) Comparison between autogenous iliac bone and freeze-dried bone allograft for repair of alveolar clefts in the presence of plasma rich in growth factors: a randomized clinical trial. J Cranio-Maxillofac Surgery 45(10):1698–1703
105. Gao S et al (2017) Comparison of glutaraldehyde and carbodiimides to crosslink tissue engineering scaffolds fabricated by decellularized porcine menisci. Mater Sci Eng C 71:891–900
106. Kargozar S et al (2017) Strontium-and cobalt-substituted bioactive glasses seeded with human umbilical cord perivascular cells to promote bone regeneration via enhanced osteogenic and angiogenic activities. Acta Biomater 58:502–514
107. Rattanawarawipa P et al (2016) Effect of lithium chloride on cell proliferation and osteogenic differentiation in stem cells from human exfoliated deciduous teeth. Tissue Cell 48(5):425–431
108. Okada H et al (2016) Plasma rich in growth factors stimulates proliferation, migration, and gene expression associated with bone formation in human dental follicle cells. J Dent Sci 11(3):245–252
109. Diaz-Gomez L et al (2014) Biodegradable electrospun nanofibers coated with platelet-rich plasma for cell adhesion and proliferation. Mater Sci Eng C 40:180–188
110. Trivedi S et al (2020) A quantitative method to determine osteogenic differentiation aptness of scaffold. J Oral Biol Craniofacial Res 10(2):158–160
111. Prins H-J et al (2014) In vitro induction of alkaline phosphatase levels predicts in vivo bone forming capacity of human bone marrow stromal cells. Stem Cell Res 12(2):428–440
112. Shahin-Shamsabadi A et al (2018) Mechanical, material, and biological study of a PCL/bioactive glass bone scaffold: importance of viscoelasticity. Mater Sci Eng C 90:280–288
113. Cai Y et al (2015) Degradability, bioactivity, and osteogenesis of biocomposite scaffolds of lithium-containing mesoporous bioglass and mPEG-PLGA-b-PLL copolymer. Int J Nanomed 10:4125
114. Mousa M et al (2021) The role of lithium in the osteogenic bioactivity of clay nanoparticles. Biomater Sci 9(8):3150–3161
115. Satija NK et al (2013) High throughput transcriptome profiling of lithium stimulated human mesenchymal stem cells reveals priming towards osteoblastic lineage. PLoS ONE 8(1):e55769
116. Zhou W et al (2022) Scaffolds of bioactive glass (Bioglass®) combined with recombinant human bone morphogenetic protein -9 (rhBMP-9) for tooth extraction site preservation. Heliyon 8(1):e08796
117. Segredo-Morales E et al (2018) Bone regeneration in osteoporosis by delivery BMP-2 and PRGF from tetronic–alginate composite thermogel. Int J Pharm 543(1–2):160–168
118. Hutchings G et al (2020) Bone regeneration, reconstruction and use of osteogenic cells; from basic knowledge, animal models to clinical trials. J Clin Med 9(1):139
119. Carbonare LD, Innamorati G, Valenti MT (2012) Transcription factor Runx2 and its application to bone tissue engineering. Stem Cell Rev Rep 8(3):891–897

120. Amarasekara DS, Kim S, Rho J (2021) Regulation of osteoblast differentiation by cytokine networks. Int J Mol Sci 22(6):2851
121. Li L et al (2017) Acceleration of bone regeneration by activating Wnt/β-catenin signalling pathway via lithium released from lithium chloride/calcium phosphate cement in osteoporosis. Sci Rep 7(1):45204
122. Jo S et al (2019) Regulation of osteoblasts by alkaline phosphatase in ankylosing spondylitis. Int J Rheum Dis 22(2):252–261
123. Allan EH et al (2003) Differentiation potential of a mouse bone marrow stromal cell line. J Cell Biochem 90(1):158–169
124. Yamamoto K et al (2015) Direct conversion of human fibroblasts into functional osteoblasts by defined factors. Proc Natl Acad Sci 112(19):6152–6157
125. Zainabadi K, Liu CJ, Guarente L (2017) SIRT1 is a positive regulator of the master osteoblast transcription factor, RUNX2. PLoS ONE 12(5):e0178520
126. Mazzoni E et al (2021) Enhanced osteogenic differentiation of human bone marrow-derived mesenchymal stem cells by a hybrid hydroxylapatite/collagen scaffold. Front Cell Dev Biol 8:610570
127. Takahashi T et al (2005) Autoregulatory mechanism of Runx2 through the expression of transcription factors and bone matrix proteins in multipotential mesenchymal cell line, ROB-C26. J Oral Sci 47(4):199–207
128. Singh A et al (2018) Role of osteopontin in bone remodeling and orthodontic tooth movement: a review. Prog Orthod 19(1):18–18
129. Ling Z et al (2017) Increased Runx2 expression associated with enhanced Wnt signaling in PDLLA internal fixation for fracture treatment. Exp Ther Med 13(5):2085–2093
130. Dong M et al (2016) Biological silicon stimulates collagen type 1 and osteocalcin synthesis in human osteoblast-like cells through the BMP-2/Smad/RUNX2 signaling pathway. Biol Trace Elem Res 173(2):306–315
131. Deng C et al (2018) Bioactive scaffolds with Li and Si ions-synergistic effects for osteochondral defects regeneration. Appl Mater Today 10:203–216
132. Anitua E et al (2013) Plasma rich in growth factors promotes bone tissue regeneration by stimulating proliferation, migration, and autocrine secretion in primary human osteoblasts. J Periodontol 84(8):1180–1190
133. Liu L et al (2019) Lithium-containing biomaterials stimulate bone marrow stromal cell-derived exosomal miR-130a secretion to promote angiogenesis. Biomaterials 192:523–536
134. Alberro A et al (2021) Extracellular vesicles in blood: sources, effects, and applications. Int J Mol Sci 22(15):8163
135. Rui S et al (2021) Comparison and investigation of exosomes derived from platelet-rich plasma activated by different agonists. Cell Transpl 30:09636897211017833
136. Zhai M et al (2020) Human mesenchymal stem cell derived exosomes enhance cell-free bone regeneration by altering their miRNAs profiles. Adv Sci 7(19):2001334
137. Liu Y, Ma Y (2019) Exosomes: a novel therapeutic agent for cartilage and bone tissue regeneration. Dose-Response 17(4):1559325819892702
138. Al-Sowayan B, Alammari F, Alshareeda A (2020) Preparing the bone tissue regeneration ground by exosomes: from diagnosis to therapy. Molecules 25(18):4205
139. Li F et al (2022) Engineering stem cells to produce exosomes with enhanced bone regeneration effects: an alternative strategy for gene therapy. J Nanobiotechnol 20(1):135
140. Guo W et al (2017) Characterization of the mechanical behaviors and bioactivity of tetrapod ZnO whiskers reinforced bioactive glass/gelatin composite scaffolds. J Mech Behav Biomed Mater 68:8–15